

Design and implementation of a torque-enhancement 2-axis magnetostatic SOI optical scanner

Tsung-Lin Tang¹, Chia-Pao Hsu¹, Wen-Chien Chen¹ and Weileun Fang^{1,2,3}

¹ Power Mechanical Engineering Department, National Tsing Hua University, Hsinchu 30013, Taiwan, Republic of China

² NEMS Institute, National Tsing Hua University, Hsinchu 30013, Taiwan, Republic of China

E-mail: fang@pme.nthu.edu.tw

Received 12 October 2009, in final form 7 December 2009

Published 18 January 2010

Online at stacks.iop.org/JMM/20/025020

Abstract

This study demonstrates the torque-enhancement design for a 2-axis magnetostatic SOI scanner driven by a double-side electroplating ferromagnetic film. The present design has two merits: (1) the slender ferromagnetic material patterns with higher length-to-width ratio enhance the magnetization, (2) the backside electroplating of the ferromagnetic film increases the volume of the ferromagnetic materials. This study also establishes the fabrication processes to implement the proposed design. The processes also have two merits: (1) the handle-layer of the SOI wafer is exploited as the shadow mask to pattern the seed-layer at the backside of the device layer, (2) the device layer of the SOI wafer acts as the cathode to enable simultaneous double-side electroplating. In applications, a 2-axis SOI scanner was implemented and characterized. Measurements show a 149% torque enhancement from the double-side electroplating design. The vertical slender ferromagnetic material patterns further increase the magnetostatic torque to 211%. This study also successfully demonstrates the Lissajous scanning using the presented 2-axis SOI scanner.

(Some figures in this article are in colour only in the electronic version)

1. Introduction

According to the characteristics of smaller feature size and lower power consumption, the micro optical scanner has demonstrated its potential for improving the performances of optical systems. There are many applications of micro scanners to date, for instance, the head-up display [1], the laser printer [2] and the optical switch [3]. After combining with image sensors, micro optical scanners can find even more applications for various optical devices, such as bar code reader [4], spectrometer [5], con-focal microscope [6] and endoscopy [7]. The silicon-based batch-fabricated micromachining process is considered as a promising technology to implement micro optical scanners. For example, surface micromachining technology has been extensively exploited to implement micro

scanners [8–10]. However, additional mechanical structures, actuators and micro assembly techniques are required to improve the moving space. Moreover, the stiffness of the thin-film mirror plate is another design consideration to prevent unwanted deformation [10]. Presently, the scanner has also been extensively implemented on the SOI (silicon on insulator) wafer [11, 12] because of the simple fabrication process and the superior material properties of single crystal silicon. The stiffness and flatness of the mirror plate are significantly improved.

In general, the electrostatic and electromagnetic forces are two major approaches to drive the SOI scanner [11, 12]. The vertical comb electrode has frequently been employed to introduce the electrostatic force to excite the SOI scanner. However, electrical isolation between electrodes needs to be considered [13], and the process to fabricate the vertical comb electrodes is not straightforward [14]. The Lorentz force is the

³ Author to whom any correspondence should be addressed.

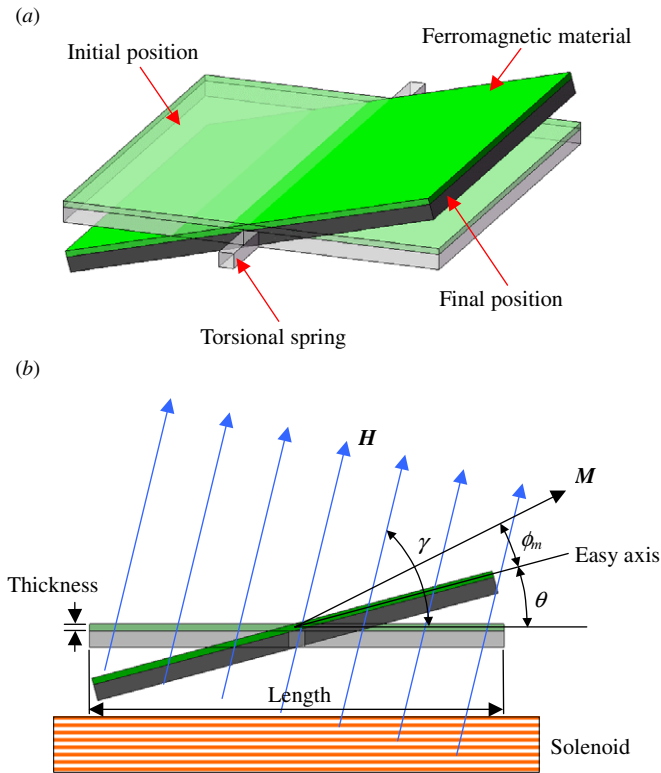


Figure 1. Actuation concepts of the scanner driven by the magnetostatic force.

most popular approach to move the electromagnetic scanner [12], and a large scan angle can be achieved. In this regard, the processes to realize the coils and the electrical routings are required [12]. The joule heat induced by the input current during the driving of the scanner is also a concern [15]. On the other hand, the electromagnetic scanner can also be driven by the magnetostatic force [16]. The magnetostatic force can be easily induced by coating a ferromagnetic material [17]. Thus, the coils and complicated electrical routings are not required, and the fabrication processes are relatively simple. However, it remains a challenge to increase the driving force as well as the scan angle for the scanner driven by the magnetostatic force.

This study presents a torque-enhancement design to increase the scan angle of a SOI scanner with ferromagnetic material coating. This SOI scanner is driven by the magnetostatic force. In short, this study patterns the ferromagnetic material to slender rectangles to increase the magnetization [18], and further employs the double-side electroplating method reported in [19] to increase the volume of the ferromagnetic materials. Thus, the magnetostatic force induced by the ferromagnetic material on the SOI scanner is significantly increased, so that the scan angle of the scanner is improved. This study also establishes the fabrication processes to realize the torque-enhancement scanner designs on the SOI wafer. The fabrication and testing results demonstrate the feasibility of the proposed design concept.

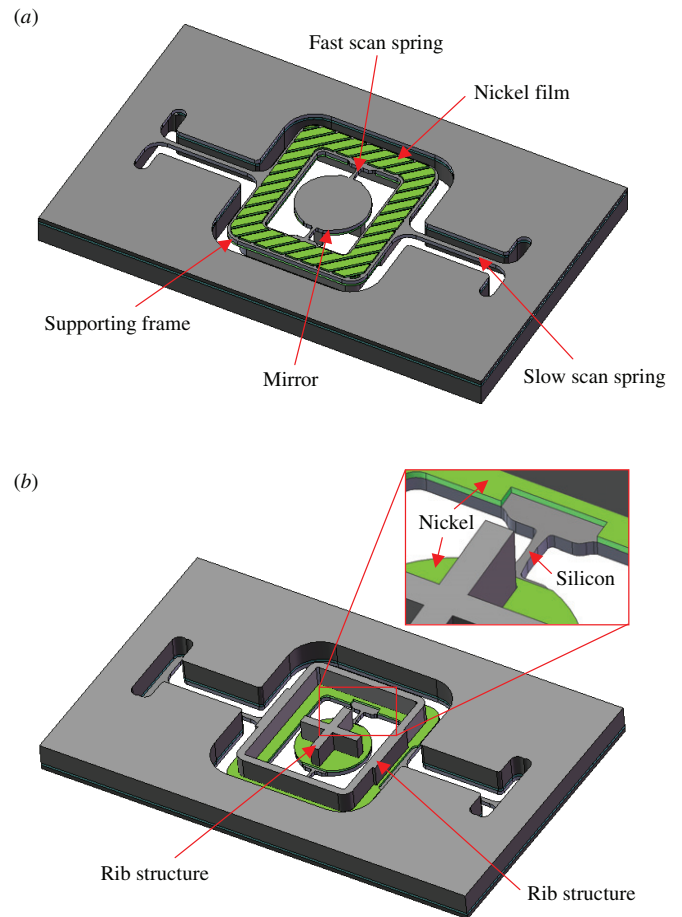


Figure 2. (a) Front-side, and (b) backside views of the scanner designed on the SOI wafer.

2. Concept and design

Figure 1(a) shows the typical 1-axis magnetostatic scanner consisted of a pair of torsional springs and a mirror plate, and the mirror plate covered with ferromagnetic material. The magnetostatic force can be induced by the interaction of ferromagnetic material and the magnetic field to drive the scanner [16]. As shown in figure 1(b), after applying a current into the solenoid to generate the magnetic field \mathbf{H}_{ext} on the magnetostatic scanner with an angle γ , the scanner will be driven by a magnetostatic torque \mathbf{T} :

$$\mathbf{T} = V_{\text{mag}} \cdot \mathbf{M} \times \mathbf{H}_{\text{ext}} \quad (1)$$

where V_{mag} is the volume of the ferromagnetic materials, and \mathbf{M} is the magnetization. Since the scanner is supported by the torsional springs of stiffness K_{θ} , the angular motion θ of the scanner resulted from the magnetostatic torque \mathbf{T} is expressed as

$$\theta = \mathbf{T} / K_{\theta}. \quad (2)$$

According to equation (1), the magnetostatic torque can be enhanced by increasing V_{mag} and \mathbf{M} . In addition, the magnetization of the ferromagnetic material is significantly

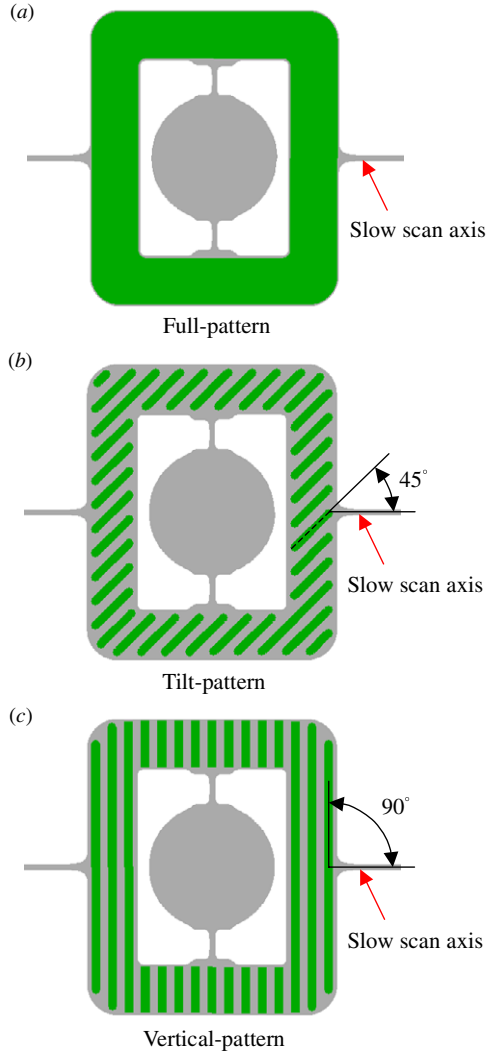


Figure 3. Different electroplated Ni patterns, (a) conventional full-pattern design, and slender rectangle designs which (b) tilt, and (c) are vertical to the scan axis.

influenced by its dimensions [17]. For soft magnetic materials, the magnetization M can be expressed as

$$M \approx \min \left[\frac{\mu_0 H_{\text{ext}} \cos(\gamma - \phi_m - \theta)}{(N_l^2 \cos^2 \phi_m + N_t^2 \sin^2 \phi_m)^{1/2}}, M_s \right] \quad (3)$$

where ϕ_m is the angle between the direction of M and the easy axis as indicated in figure 1(b), and M_s is the saturation magnetization. Moreover, N_l and N_t are respectively the shape-anisotropy coefficients along the length and the thickness. For a rectangular pattern, the shape-anisotropy coefficient is smaller along the long-axis direction; thus, the magnetization is larger along the long-axis direction [17].

2.1. Torque enhancement by increasing M

This study exploits the concept in equation (1) to design the torque-enhancement magnetostatic 2-axis SOI scanner by increasing V_{mag} and M . This study further establishes the fabrication processes to implement the torque-enhancement

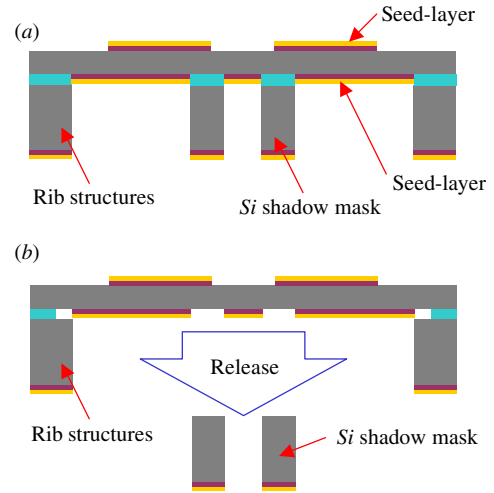


Figure 4. Schematic of the method to pattern the seed-layer on the backside of the device, (a) before and (b) after releasing the shadow mask. The handling silicon layer acted as the shadow mask during patterning of the seed-layer.

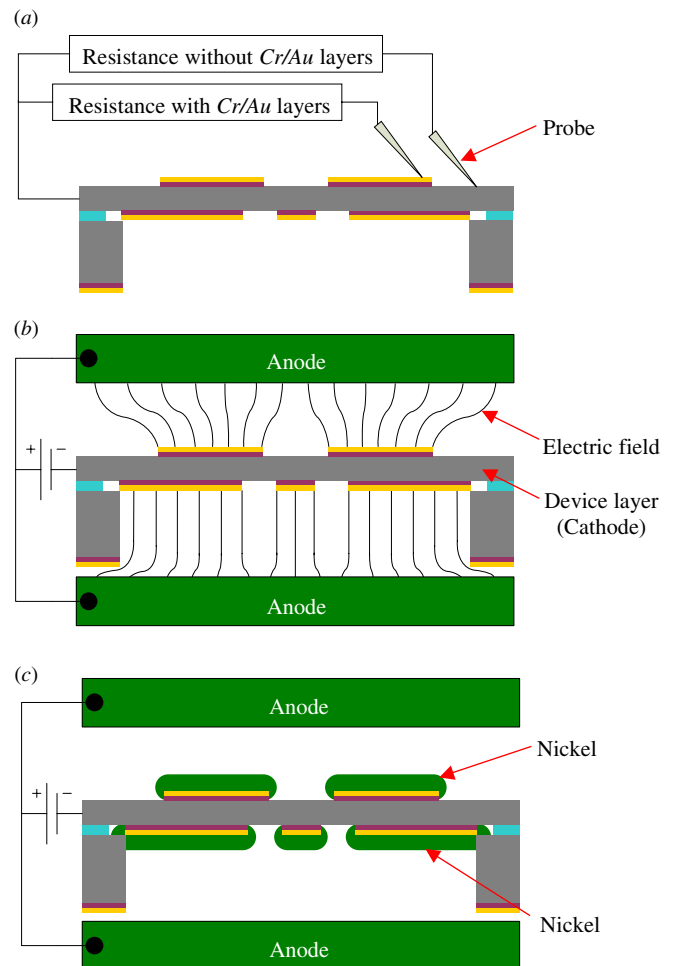


Figure 5. Schematic of double-side electroplating, (a) characterization of the resistance, (b) distribution of the magnetic field and (c) after electroplating. The device Si layer acted as the cathode during electroplating.

scanner design on the SOI wafer. The thickness of the device-layer, buried oxide layer and handle-layer are $40 \mu\text{m}$, $2 \mu\text{m}$

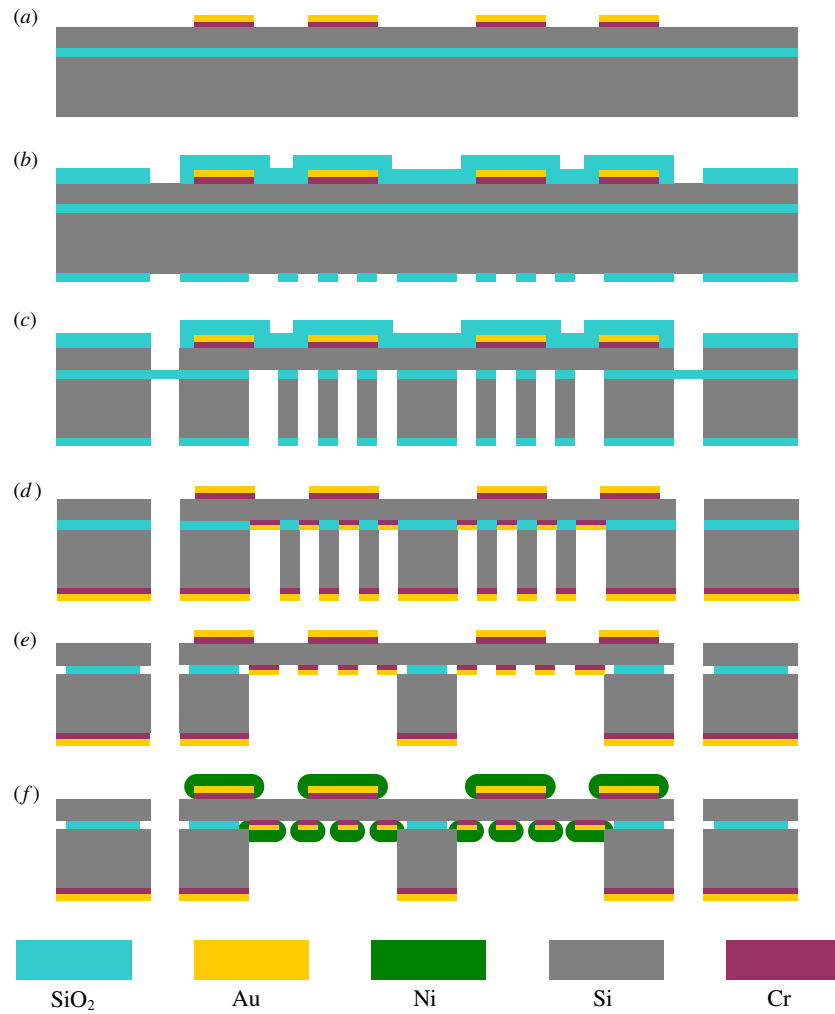


Figure 6. Fabrication process steps.

and $370 \mu\text{m}$, respectively. Figure 2 illustrates the schematic design of the SOI scanner. Figure 2(a) shows the front-side view of the 2-axis scanner made of the device Si layer of the SOI wafer. The scanner consists of mirror, torsional springs and supporting frame. The radius of the mirror plate is $625 \mu\text{m}$. The slow scan spring is $1800 \mu\text{m}$ long and $41 \mu\text{m}$ wide, and the fast scan spring is $300 \mu\text{m}$ long and $50 \mu\text{m}$ wide. The internal dimensions of the supporting frame are $1490 \mu\text{m} \times 1956 \mu\text{m}$, and the width of the frame is $500 \mu\text{m}$. In addition, the radii of the round corners for slow scan springs and fast scan springs are $100 \mu\text{m}$ and $45 \mu\text{m}$, respectively. The Ni film is electroplated on the supporting frame for magnetic actuation. As indicated in figure 2(a), the topside of the Ni film is patterned to slender rectangles to increase the shape anisotropy so as to further enhance M . In comparison, this study has respectively designed three different types of Ni patterns on the top surface of the supporting frame, as shown in figure 3. Figure 3(a) shows the supporting frame of a 2-axis scanner fully covered with the Ni film (named full-pattern) [16]. Figures 3(b) and (c) show the supporting frames respectively covered with 45° (named tilt-pattern) and 90° (named vertical-pattern) slender Ni patterns to the slow

scan axis. This study will also investigate the variation of magnetization strength with the angle of slender pattern.

2.2. Torque enhancement by increasing V_{mag}

Figure 2(b) shows the backside view of the scanner, and the rib structures made of the handling Si layer are employed to increase the stiffness of mirror and supporting frame. As indicated in figure 2(b), the Ni film is selectively electroplated at the backside of the mirror and supporting frame to increase the V_{mag} . However, the backside of flexible torsional spring is not plated with the Ni film to prevent unwanted deformation due to the residual stress of the electroplated film and the thermal mismatch between the Si and metal layer. In addition, the de-lamination and fatigue of the Ni film due to the cycling loads on the torsional spring are other considerations for the bi-material spring. This study further establishes the fabrication processes to realize the selective electroplating at the backside of the SOI wafer. As shown in figure 4(a), the handling Si layer is employed as the shadow mask to define the patterns of the seed-layer at the backside of the scanner. After that, the Si shadow mask can easily be removed by undercutting of the buried oxide, as shown in figure 4(b). Thus, the complicated

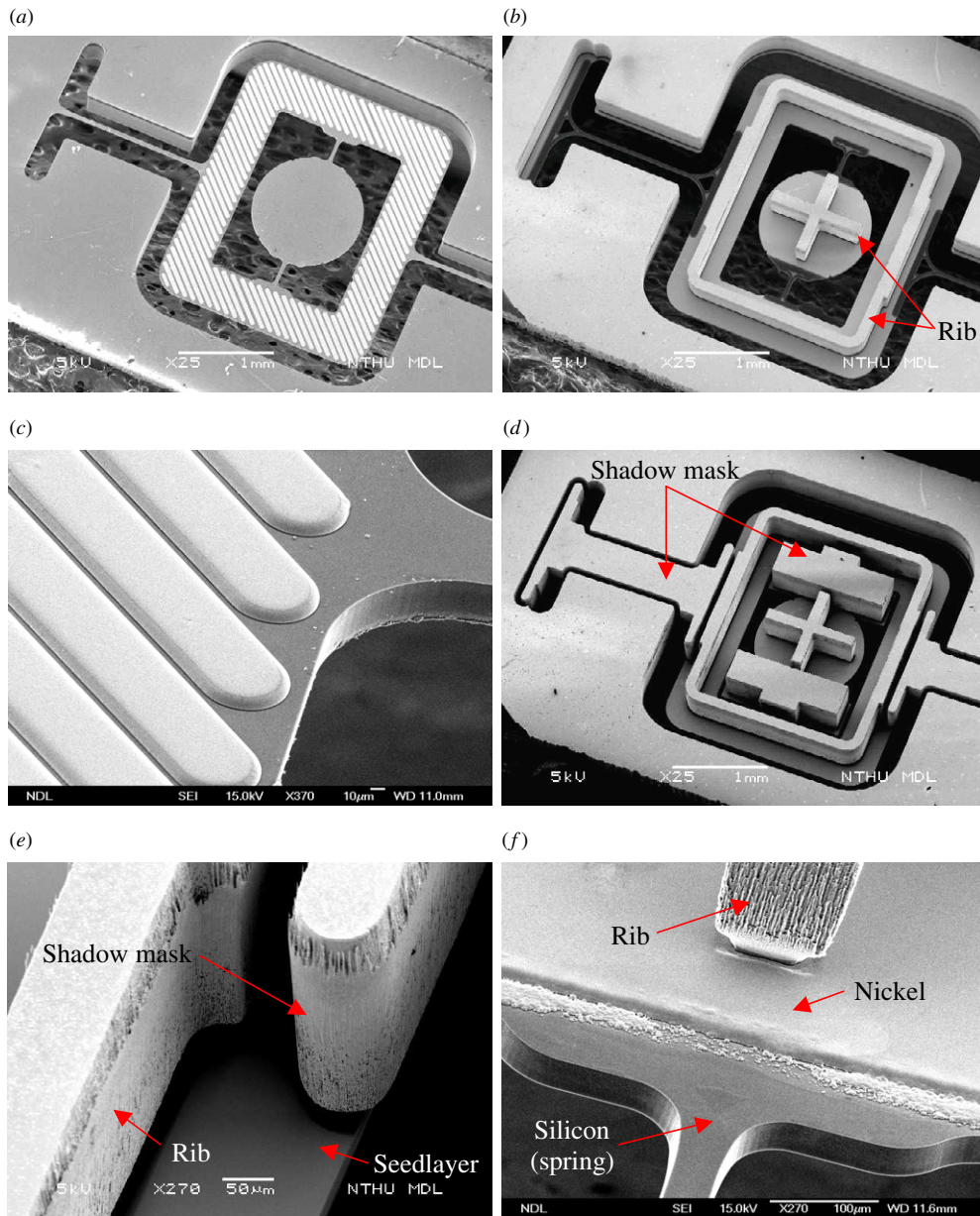


Figure 7. The SEM micrographs of (a), (b) front side and backside of a typical fabricated scanner, (c) tilt electroplated slender Ni patterns, (d) before releasing the Si shadow mask, (e) seed-layer was patterned by silicon shadow mask and (f) selectively plated Ni pattern at the backside of the scanner.

process to pattern the seed-layer on the backside of the SOI device Si layer is prevented. As shown in figure 5, this study further employs the low-resistivity device Si layer as the cathode for double-side electroplating. As characterized using the setup in figure 5(a), the resistance of Si without and with Cr/Au layers is respectively 2.23 MΩ and 50 kΩ. Thus, the resistance of Si drops only 2.2% after depositing with Cr/Au layers. The lower resistance of Si with Cr/Au layers is caused by the metal–semiconductor contact. Figure 5(b) shows the setup for double-side electroplating, which indicates that the current is mainly distributed on Si with Cr/Au layers. Since the resistances of Si and the Cr/Au seed-layers are different, the ferromagnetic materials can be selectively electroplated on the device Si layer by

choosing a proper current density (~0.02 ASD), as shown in figure 5(c).

3. Fabrication and results

Figure 6 shows the process integration to realize the presented micro scanner. This study employed an SOI wafer of the low-resistivity device Si layer (0.03 Ω cm) for the process. As shown in figure 6(a), the Cr/Au seed-layers were deposited and patterned to define the slender patterns on the front side of the device layer. After that, SiO₂ was deposited and patterned as the hard-mask for the following DRIE, as illustrated in figure 6(b). DRIE (deep reactive ion etching) was then employed to define the in-plane shape of structures, as shown in figure 6(c). After stripping the SiO₂ hard-mask and the

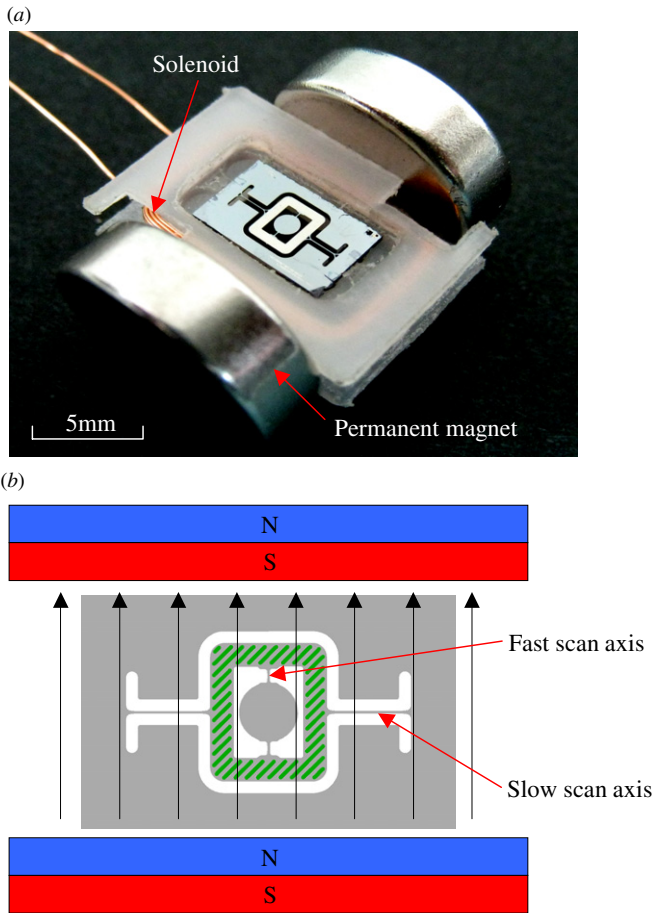


Figure 8. (a) The driving stage established in this study, and (b) the top view of the scanner in the magnetic field.

buried oxide layer by HF, the seed-layer was deposited by E-gun and then patterned by the silicon shadow mask, as shown in figure 6(d). The silicon shadow mask was made of the patterned handling Si layer at the backside of the SOI wafer. Generally, it was difficult to pattern the seed-layer at the backside of the mirror by photolithography. As shown in figure 6(e), the silicon shadow mask was removed after the

undercut of buried oxide by HF. Finally, the ferromagnetic material was simultaneously electroplated on both sides of the device layer, as shown in figure 6(f).

The SEM (scanning electron microscope) micrographs in figures 7(a) and (b) respectively show the front side and the backside of a typical fabricated scanner. The mirror, supporting frame, torsional springs and ribs are observed. The front side of the supporting frame contains the electroplated Ni with tilt-pattern design. In addition, the backside of mirror and supporting frame also contain the electroplated Ni film. The average thickness of the Ni film is 13 μm . The zoom-in SEM micrograph in figure 7(c) demonstrates the distribution of tilt slender Ni patterns, and these Ni patterns are selectively electroplated on the supporting frame. The micrograph in figure 7(d) shows the backside view of the scanner before the removal of the silicon shadow mask (related to the process in figure 6(d)). It is clearly observed that the torsional springs are covered with the silicon shadow mask. Moreover, the zoom-in SEM micrograph in figure 7(e) shows the Cr/Au seed-layers patterned by the silicon shadow mask. As shown in the zoom-in micrograph of figure 7(f), the Ni film selectively electroplated on the backside of mirror but not spring is demonstrated (associated with the process in figure 6(f)).

4. Experiments and discussions

The driving stage in figure 8 is established in this study for scanning tests. As shown in figure 8(a), the chip with a 2-axis SOI scanner is fixed to the stage. The permanent magnets (with $B = 0.30$ tesla) ensure the magnetization direction of ferromagnetic material, and the strength of the magnetic field in the center of this stage is 18.02 kA m^{-1} . The solenoid embedded in the stage provides the magnetic field to drive the scanner. Thus, the orientation of the permanent magnets and the slow scan axis of the mirror are fixed, as indicated in figure 8(b). Nevertheless, the scanners with different Ni patterns shown in figure 3 were characterized in the tests. As a dc current was applied to the solenoid, the scanner was driven by a constant magnetic field and yielded a static

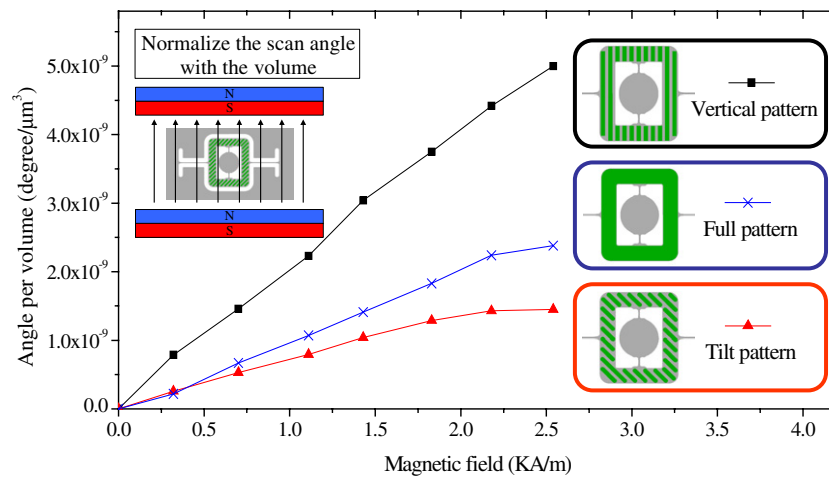


Figure 9. The scan angle (normalized to the volume of the Ni film) driven by the magnetostatic torque induced from different Ni patterns.

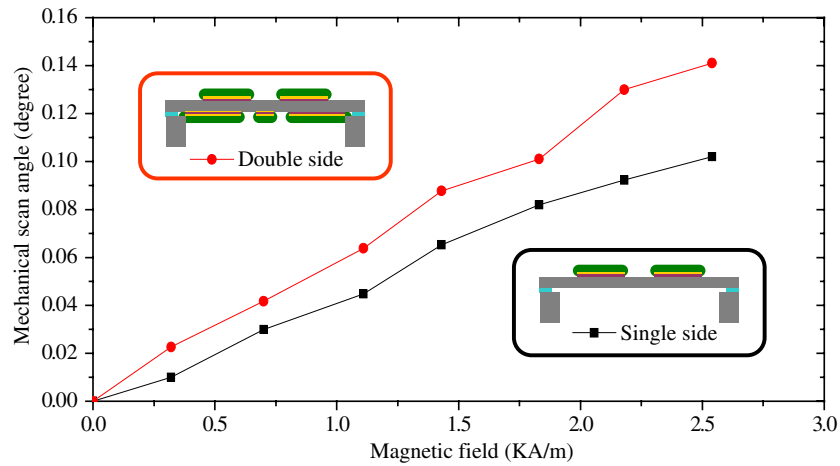


Figure 10. The scan angle driven by the magnetostatic torque induced from the single-side and the double-side electroplating scanners.

angular displacement. In other words, the input dc current was employed to modulate the strength of the magnetic field and further tune the scan angle of the slow scan axis. The measurements in figure 9 show the mechanical scan angle (driven by the magnetic field yielded from the dc current) per unit volume of Ni for scanners with different ferromagnetic material patterns indicated in figure 3. Thus, the effect of ferromagnetic material pattern on the magnetization strength M can be evaluated. Since the total volume of ferromagnetic material also varies with the pattern in figure 3, this study normalizes the measured scan angle with the volume of ferromagnetic material. As compared with the conventional full-pattern design (in figure 3(a)), the vertical-pattern design (in figure 3(c)) increases the magnetostatic torque 211%. As for the tilt-pattern design in figure 3(b), the direction of the magnetic field is not identical with its long axis. In addition, the tilt rectangle pattern has a smaller aspect ratio (length/width). Thus, the Ni film with tilt-pattern design has the smallest scan angle per volume.

The measurement results in figure 10 respectively show the mechanical scan angle of the slow scan axis (also driven by the magnetic field yielded from the dc current) induced by the single-side and double-side electroplating designs. According to equation (2), the magnetostatic torque is proportional to the mechanical scan angle θ . Therefore, the results reveal an average of 149% enhancement of the magnetostatic torque from the double-side electroplating design. According to the measurement, the volume of the double-side electroplated Ni was increased 162%. It demonstrates the double-side electroplating technique successfully increases the volume of ferromagnetic materials, and further increases the driving torque on the scanner.

In application, this study also demonstrates the Lissajous scanning using the presented 2-axis SOI scanner. As shown in figure 11(a), a typical fabricated scanner (containing double-side electroplated Ni layers with tilt-pattern design at the front-side surface) is also fixed to the driving stage with embedded solenoid. The permanent magnets (with $B = 0.30$ tesla) are arranged to cause the magnetization direction of ferromagnetic material to have a tilt angle with the slow scan axis. In

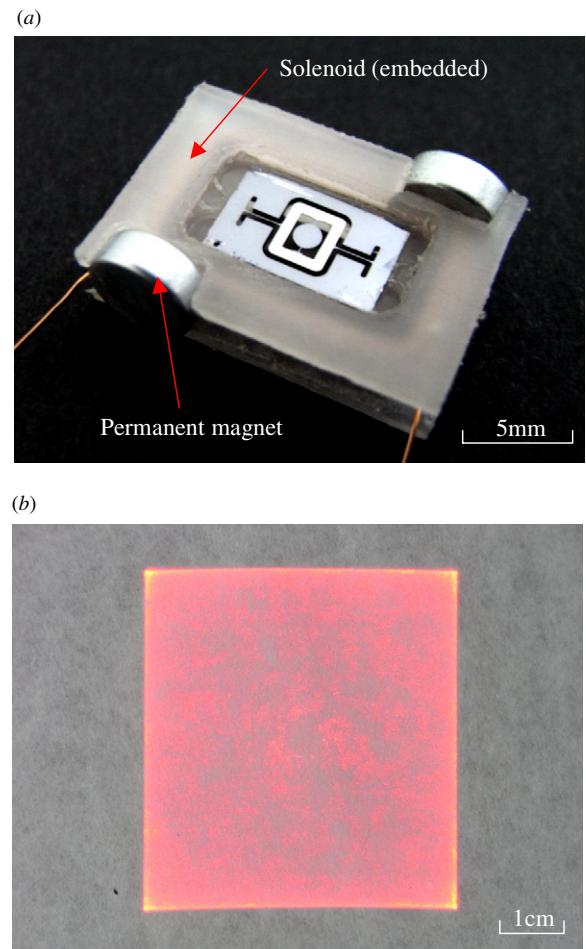


Figure 11. Driving the magnetostatic 2-axis scanner. (a) Driving stage, (b) typical 2D scan pattern.

this case, the strength of the magnetic field in the center of the driving stage is 20.37 kA m^{-1} . Moreover, a sinusoidal current of 0.40 A (root-mean-square value) is applied to the solenoid. As a result, the scanner is driven by a sinusoidal magnetic field with amplitude of 1.05 kA m^{-1} . Thus, the torque induced by the sinusoidal magnetic field will apply

on both axes of the scanner, and then lead to the 2-axis scan pattern. The typical 2D scan pattern is shown in figure 11(b). As shown in figure 11, the dimensions of the 2D image on screen are 5.8 cm (vertical) \times 4.8 cm (horizontal). The distance between the screen and the scanner is 25 cm. The slow scan and fast scan of this 2-axis scanner were respectively operated at 584 Hz (with an optical scan angle of 13.2° in vertical direction) and 111 49 Hz (with optical scan angle of 11.0° in horizontal direction). In this design, the quality factors of the slow and fast scan axes are respectively 119 and 799 at 1 atm. According to [20], the resolution of the Lissajous pattern generated by this scanner is 429 \times 429 pixels with a refresh rate of 48.72 Hz.

5. Conclusions

This study presents the concepts of the torque-enhancement design for the 2-axis magnetostatic SOI scanner. The double-side electroplated Ni layers and the slender ferromagnetic patterns are respectively employed to increase the V_{mag} and M . Thus, the driving force for the 2-axis magnetostatic SOI scanner is significantly improved. The micro fabrication processes, including the silicon shadow mask and the simultaneous electroplating on both sides of the device Si layer, have also been established to implement the present design. The measurement results show that the slender Ni patterns will lead to an additional 211% torque enhancement, as compared with the conventional full-pattern design. Moreover, the double-side electroplating approach has a 149% torque enhancement. In applications, this study successfully demonstrates the Lissajous scanning using the presented 2-axis SOI scanner.

Acknowledgments

This paper is based (in part) on work supported by the National Science Council, Taiwan under grant NSC 96-2628-E-007-008-MY3 and by the Ministry of Economic Affairs, Taiwan, under contract no 97-EC-17-A-07-S1-011. The authors would like to express their appreciation to the Nano Science and Technology Center of National Tsing Hua University, and Nano Facility Center of National Chiao Tung University in providing the fabrication facilities.

References

- [1] Sprague R, Montague T and Brown D 2005 Bi-axial magnetic drive for scanned beam display mirrors *Proc. SPIE* **5721** 1–13
- [2] Davis W O, Brown D, Helsel M, Sprague R, Gibson G, Yalcinkaya A and Urey H 2007 High-performance silicon scanning mirror for laser printing *Proc. SPIE* **6466** 64660D
- [3] Chu P B, Lee S-S and Park S 2002 MEMS: the path to large optical crossconnects *Commun. Mag.* **40** 80–7
- [4] Yalcinkaya A D, Ergeneman O and Urey H 2007 Polymer magnetic scanners for bar code applications *Sensors Actuators A* **135** 236–43
- [5] Ataman Ç and Urey H 2008 Magnetic actuated FR4 scanners for compact spectrometers *Proc. SPIE* **6993** 699303
- [6] Miyajima H, Asaoka N, Isokawa T, Ogata M, Aoki Y, Imai M, Fujimori O, Katashiro M and Matsumoto K 2003 A MEMS electromagnetic optical scanner for a commercial confocal laser scanning microscope *J. Microelectromech. Syst.* **12** 243–51
- [7] Chong C, Isamoto K and Toshiyoshi H 2006 Optically modulated MEMS scanning endoscope *Photonics Technol. Lett.* **18** 133–5
- [8] Kiang M-H, Solgaard O, Lau K Y and Muller R S 2002 Electrostatic combdrive-actuated micromirrors for laser-beam scanning and positioning *J. Microelectromech. Syst.* **7** 27–37
- [9] Fan L and Wu M C 1998 Two-dimensional optical scanner with large angular rotation realized by self-assembled micro-elevator *Broadband Optical Networks and Technologies (Monterey, CA, July 1998)* pp 107–8
- [10] Wu M and Fang W 2005 Design and fabrication of MEMS devices using the integration of MUMPs, trench-refilled molding, DRIE and bulk silicon etching processes *J. Micromech. Microeng.* **15** 535–42
- [11] Ji C-H, Choi M, Kim S-C, Lee S-H, Kim S-H, Yee Y and Bu J-U 2006 An electrostatic scanning micromirror with diaphragm mirror plate and diamond-shaped reinforcement frame *J. Micromech. Microeng.* **16** 1033–9
- [12] Jeong H-M, Park Y-H, Cho Y-C, Hwang J, Chang S-M, Kang S-J, Jeong H-K, Kim J O and Lee J-H 2009 Slow scanning electromagnetic scanner for laser display *Proc. SPIE* **7** 043003
- [13] Schenk H, Dürr P, Kunze D, Lakner H and Kück H 2001 A resonantly excited 2D-micro-scanning-mirror with large deflection *Sensors Actuators A* **89** 104–11
- [14] Hah D, Choi C-A, Kim C-K and Jun C-H 2004 A self-aligned vertical comb-drive actuator on an SOI wafer for a 2D scanning micromirror *J. Micromech. Microeng.* **14** 1148–56
- [15] Mitsui T, Takahashi Y and Watanabe Y. 2006 A 2-axis optical scanner driven nonresonantly by electromagnetic force for OCT imaging *J. Micromech. Microeng.* **16** 2482–7
- [16] Yalcinkaya A D, Urey H and Holmstrom S 2007 NiFe plated biaxial MEMS scanner for 2-D imaging *IEEE Photonics Technol. Lett.* **19** 330–2
- [17] Judy J W and Muller R S 1996 Magnetic microactuation of torsional polysilicon structures *Sensors Actuators A* **53** 392–7
- [18] Tang T L, Chen W C, Chen R and Fang W 2008 The torque-enhancement design for magnetostatic scanner *Optical MEMS and Nanophotonics (Freiburg, Germany, August 2008)* pp 164–5
- [19] Hsu C P, Chen W C, Tang T L, Yip M C and Fang W 2008 The two-axis magnetostatic-drive single-crystal-Si micro scanner driven by back-side electroplating Ni film *Optical MEMS and Nanophotonics (Freiburg, Germany, August 2008)* pp 152–3
- [20] Roscher K-U, Grätz H, Schenk H, Wolter A and Lakner H 2004 Low-cost projection device with a 2D resonant micro scanning mirror *Proc. SPIE* **5348** 22–3